Available online at www.sciencedirect.com
ScienceDirect
Coastal Engineering 54 (2007) 717–733
Coastal Engineering
An International Journal for Coastal, Harbour and Offshore Engineers
www.elsevier.com/locate/coastaleng

Modelling of complex coastal environments: Some considerations for best practise

O.P. Jones [a,*], O.S. Petersen [b], H. Kofoed-Hansen [c]

[a] Department of Civil and Environmental Engineering, University College London, Gower Street, London, WC1E 6BT, United Kingdom
[b] Department of Coastal Engineering, DHI Water, Environment & Health, Agern Allé 5, DK-2970, Hørsholm, Denmark
[c] Department of Marine Software, DHI Water, Environment & Health, Agern Allé 5, DK-2970, Hørsholm, Denmark

Received 22 June 2006; received in revised form 6 February 2007; accepted 15 February 2007
Available online 16 July 2007

Abstract

The numerical modelling of large-scale sediment transport and coastal morphology frequently requires significant model reduction and optimisation in order to achieve expedient conclusions. This study provides a detailed sensitivity analysis of various model 'reduction' techniques using the Bristol Channel, western U.K. as a case study. The work elucidates a number of the best practises for employment of state-of-the-art systems to complex coastal regions.
© 2007 Elsevier B.V. All rights reserved.

1. Introduction

Process-based models make predictions by solving discretised empirical or Newtonian equations using numerical techniques. Therefore, the accuracy of the predictions is directly related to the sophistication of the incorporated equations. State-of-the-art systems are reliable at predicting complex hydrodynamics but application to morphodynamical simulation becomes increasingly unreliable over longer time-scales (see Leont'yev, 2003). This is a reflection of our current knowledge of longer-term processes and interactions. This study focuses on the design of a coupled modelling system, set up to improve understanding of a particularly complex coastal environment.

A number of techniques have been developed that assist the validity of process-based morphological simulations (see de Vriend et al., 1993; Latteaux, 1992). These include the use of both input and model 'reduction' techniques. In this study we focus primarily on making a contribution to the latter. Recent studies, including Sandpit (2005), tested a number of 'state-of-the-art' morphodynamic modelling systems and suggested large differences in predictions despite the similarities in the underlying equations and assumptions of each model. These differences were attributed to the varying input and model reduction approaches taken by the individual modellers.

1.1. Model reduction

Model reduction involves taking advantage of the difference in time-scales between hydrodynamic and morphological change. This helps to reduce the complexity of the model and improve the long-term efficacy. There are two main approaches to process-based model reduction. The first usually involves an increase of the morphological time-step and is employed in large coupled models. The second, sometimes referred to as 'formal model reduction', involves a more fundamental analysis of the underlying equations and assumptions that drive processes at the coastline. The subject forms a branch of modelling that is useful in understanding the processes behind cyclical morphological features. For a comprehensive review, see Hudson et al. (2005). In this study we focus on making a contribution to the former.

* Corresponding author.
E-mail addresses: o.jones@ucl.ac.uk (O.P. Jones), osp@dhigroup.com (O.S. Petersen), hkh@dhigroup.com (H. Kofoed-Hansen).

0378-3839/$ - see front matter © 2007 Elsevier B.V. All rights reserved.
doi:10.1016/j.coastaleng.2007.02.004

Increasing the morphological time-step invariably involves a combination of:

- An increase in the time-step between consecutive calls of the sediment transport/morphological models. In between the calls, the bed is updated by extrapolating incremental bed changes computed at a previous time-step by establishing relationships between the waves/flow and bathymetry. (See de Vriend et al., 1993, for further details);
- The 'Online' method. This involves multiplying the bed changes computed during one hydrodynamic time-step, by an acceleration factor (see Roelvink, 2006).

In this study the validity of using both methods in an environment subject to strong tidal and wave forcing is tested. In doing so, optimised sediment transport updating frequencies and acceleration factors are derived.

1.2. Further model reduction

Restricting the number of simulated wave conditions to only those responsible for sediment transport also helps to minimise the computational effort. This study aims first, to identify and include only wave conditions that are significant to sediment transport, and second, finding the minimum frequency at which the wave field needs to be re-computed. Additional improvement of the model efficiency is then sought by simple optimisation of the mesh geometry. This includes reductions in both the grid resolution and domain size.

1.3. The study area

The Bristol Channel is a large macro-tidal inlet in the western U.K. The region is subject to a diverse range of the wind and wave conditions and has one of the highest tidal ranges in the world. This provides the backdrop to strong wave–current interaction and complex tidal and wave-driven sediment transport.

A number of studies (Harris and Collins, 1985; Harris and Jones, 2005) have hypothesised that in spite of the ebb-dominated tidal transport, there exists a wave-induced easterly directed transport pathway providing a potential mechanism for importing marine derived sediment into the north eastern part of the central Bristol Channel.

Waves induce a time-averaged mass and momentum fluxes within fluid in which they propagate (see van Rijn, 1993). With progressively shallower water, non-linearities of the propagating waves become more pronounced and the asymmetry of the waves increases. Wave steepness increases and the waves will break generating vertical and horizontal gradients in the mass and momentum fluxes. If waves approach at an oblique angle, this excess flux is driven parallel to the coastline in the form of a long-shore current. Longuet-Higgins and Stewart (1964) explain this phenomenon using the 'radiation stress concept'. In addition to the radiation stresses, waves also affect sediment transport by increasing the near-bed orbital velocity and shear stress. The present model scope needs to include all of these wave-induced sediment transport processes as well as describing the effects of tidal currents and wave–current interaction.

1.4. Model aims

Capturing these processes within a reasonable computational time-scale requires extensive model optimisation and reduction. High resolution in the breaking zone must be offset with the need for a spatial footprint large enough to describe regional-scale transport processes.

The aim of the following experiments is to build a coupled model that a) incorporates the physics of all contributing processes and; b) is efficient enough to facilitate multiple simulations and hence capture the full range of physical processes.

2. Model design

The modelling system used is the MIKE 21 flexible mesh (FM) suite consisting of flow, spectral wave and sediment transport models. All of the models in this FM suite are based on a flexible mesh approach. In the following section we provide a brief description of each model. Inclusion of the underlying equations and more peripheral physical processes is restricted only to those adjusted in the model reduction experiments of Sections 3, 4 and 5.

2.1. Model coupling

In the coupled wave/current approach of this modelling study, the effects of wave setup and momentum gradients are incorporated by extracting the radiation stresses (S_{xx}, S_{yy} and S_{xy}) from stationary wave simulations (see Fig. 1). The resulting tensor field is then passed on to a coupled hydrodynamic/sediment transport model (henceforth, HD/ST) in which the radiation stress gradients, ($\partial S_{xx} / \partial x$, $\partial S_{yy} / \partial y$, $\partial S_{xy} / \partial y$) drive momentum and mass fluxes, promoting wave-induced currents and long-shore transport. Simulating the wave-induced sediment transport in the HD/ST model depends on the detail in which wave decay is resolved in the near-shore zone by the wave model. Resolving this correctly requires an accurate description of the near-shore bathymetry. The approach also requires the simulation of a large number of combined wave and water level conditions to capture the full range of potential wave conditions.

During the final HD/ST simulations, the sediment transport rate invoked by the effects of both wave-induced currents and tidal forcing are derived by interpolation from a pre-computed look-up table, calculated using the DHI *Sediment Transport Program* (see Section 2.4).

2.2. The wave model

The MIKE 21 SW spectral wave model includes two types of algorithm which vary in their level of sophistication. To reduce computational run times, this study uses the parametrically decoupled version of the model (henceforth DS module). The DS module solves the wave action-balance equation (see

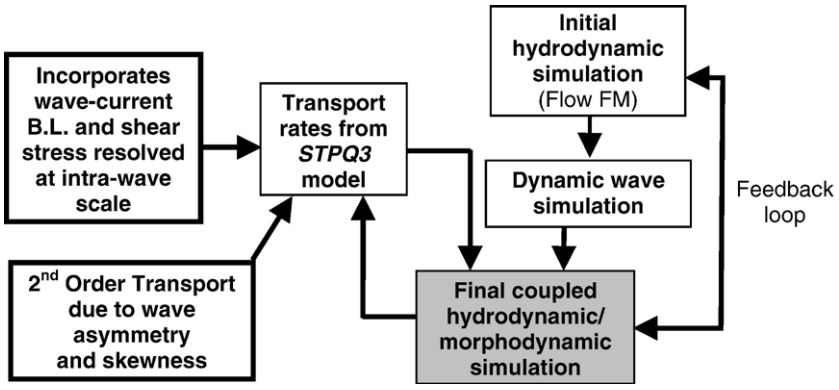

Fig. 1. Details of the model coupling procedure.

Komen et al., 1994) as a stationary or in-stationary (time dependent) solution over direction and spatial space employing two parameterisations to improve efficiency (see Section 4 for further details). Results of a validation exercise are presented comparing the performance of the DS model with real measurements from the Bristol Channel.

2.3. The flow model

The hydrodynamic model solves the two dimensional Reynolds-averaged Navier–Stokes equations invoking the approximations of Boussinesq and hydrostatic pressure. This involves continuity, momentum, temperature, salinity and density equations (DHI, 2005).

2.4. The sediment transport/morphological model

In order to capture the combined effects of wave and current action on bed shear stress and sediment transport, it is necessary to resolve the boundary layer in as much detail as possible. The physics of the boundary layer, however, becomes increasingly complicated under the combined influence of waves and currents (see Bakker and Van Doorn, 1978; Kemp and Simons, 1982). In the present study, we seek an approach that incorporates modifications to the boundary layer from orbital wave motion and also adjustments to the vertical balance of forces induced by the action of wave breaking and setup (gradients in radiation stresses).

For this purpose DHI's *Sediment Transport Program*, henceforth *STPQ3*, is employed which provides a quasi-3D description of the hydrodynamic force balance through the water column and hence an improved description of the wave–current boundary layer. The approach resolves the spatial and temporal variation of shear stress, flow velocity and sediment concentration using the integrated momentum approach of Fredsøe (1984). The main drawback with this approach is the effort required to re-compute the boundary layer characteristics at every call to the sediment transport model. Therefore to reduce this, a form of model reduction is employed in which a detailed look-up table is pre-computed for a range of wave/tide/sediment combinations that cover the conditions of the modelling study. During the simulation, sediment transport rates are interpolated from the look-up table at each call to the sediment transport model.

3. Mesh and domain optimisation

3.1. Choice of mesh size

The hydrodynamic model solves the Reynolds-averaged Navier–Stokes equation at the centre of each element in the model domain. The size and spacing of the elements determine the limits of the 'resolved' and 'unresolved' domains (Abbott and Minns, 1998). In order to incorporate the influence of the sub-grid or 'unresolved' flow on the 'resolved' flow, the model uses a turbulence closure scheme to dissipate energy from the system. Models with larger element sizes require more energy to be diffused at the sub-grid scale and hence introduce more uncertainty into their predictions. The model uses the approach of Smagorinsky (1963) to dissipate energy at scales smaller than the mesh spacing (Δx_n). The method assumes that the ability of a fluid to sustain internal shear stresses is related to the mean strain rate tensor ($\partial\overline{u}_i / \partial x_j + \partial\overline{u}_i / \partial x_j$) by a 'turbulent eddy viscosity' υ_t,

$$\tau_{ij} = \upsilon_t \left(\frac{\partial \overline{u}_i}{\partial x_j} + \frac{\partial \overline{u}_j}{\partial x_i} \right) \tag{1}$$

υ_t is computed as a function of a characteristic length scale, h, based on the mesh spacing,

$$h = [(2\Delta x_1)(2\Delta x_2)(2\Delta x_3)]^{1/3} \tag{2}$$

and is itself a function of the intensity of the rate of shearing in the fluid ($\overline{S}$)

$$\upsilon_t = (a_1)^2 h^2 \overline{S}^{1/2} \tag{3}$$

Eq. (3) suggests that the turbulent eddy viscosity tends to zero as the second power of the grid size. The shear stress (τ_{ij}) and, therefore, the sub-grid energy removed from the system also tend to zero with the second power of the grid size. As the

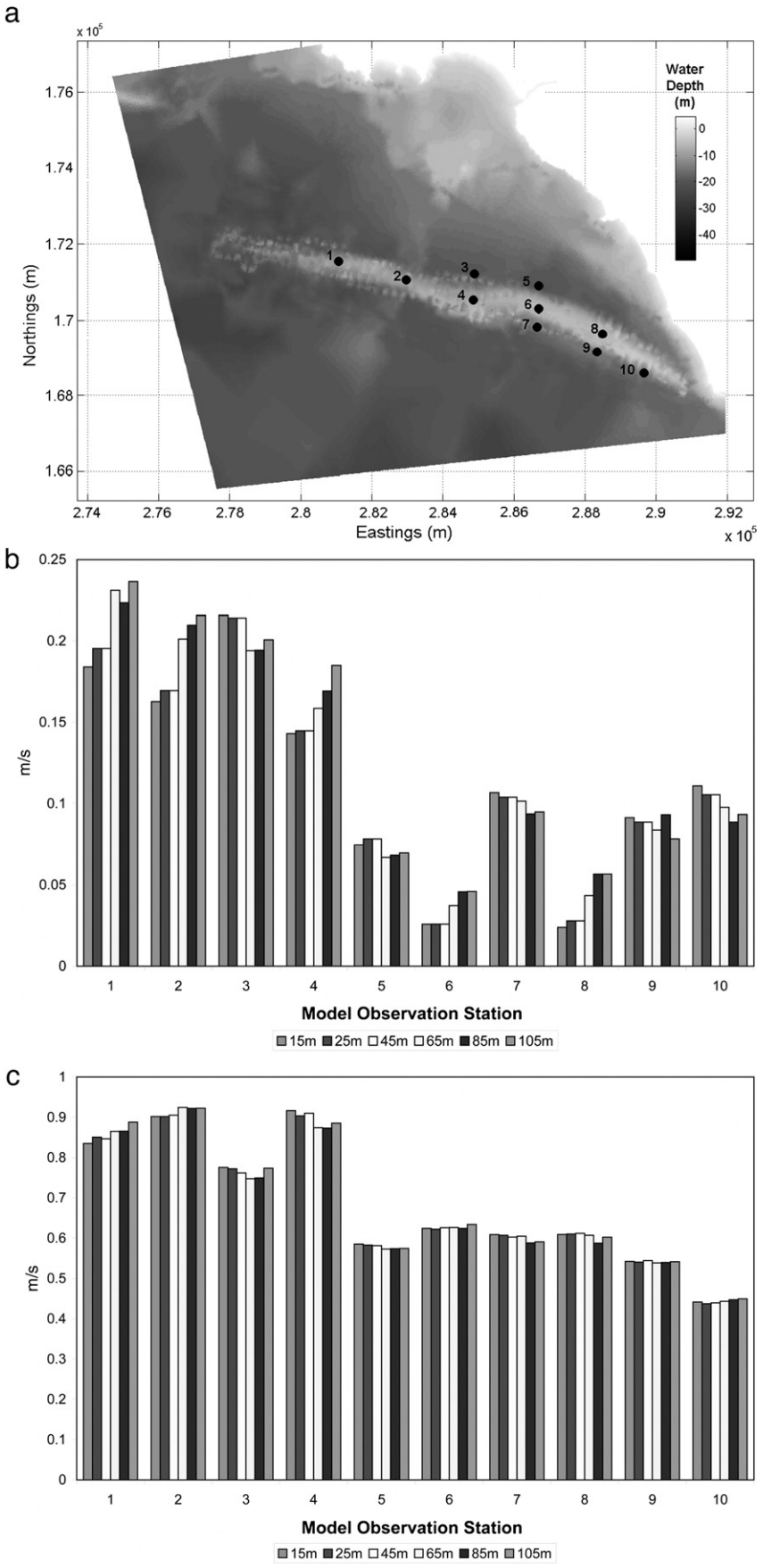

Fig. 2. (a) Region selected for grid resolution tests including positions of model observation points. Predicted: (b) mean and; (c) instantaneous current speed standard deviation over 4 h at 10 model observation points for all 6 grid resolutions.

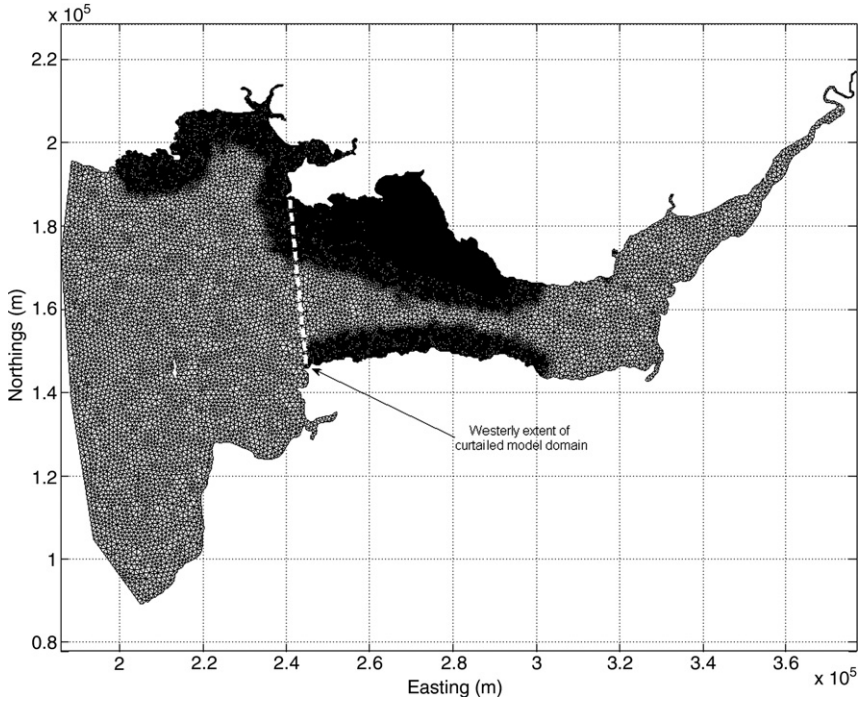

Fig. 3. Larger regional mesh, initially constructed for the complete modelling study. Figure includes the western boundary of the curtailed mesh, proposed for optimising model CPU time.

grid spacing gets smaller, the diffusive effect of the turbulence closure scheme reduces. Ideally the turbulence closure scheme should dissipate energy to the same extent as infinitesimally small grid spacing. However, this is not the case, due mainly to the selection of the constant, a_1. In highly variable flow fields, it is unclear what value to assign for a_1 and the sub-grid energy dissipation is miscalculated.

The purpose of the following experiment was to find, under dynamic forcing conditions, a grid resolution in which the turbulence closure scheme is not invalidated by the assumptions described above. A constant $a_1 = 0.28$ was used in all tests and grid of 15 m, 25 m, 45 m, 65 m and 85 m and 105 m. For the model domain, a region around the Nash Sands in the central Bristol Channel is isolated (see Fig. 2 (a)), and using each grid in turn, a tidal range of 8 m is applied at the western boundary. Velocity measurements are recorded at 10 observation positions inside the model (positions indicated in Fig. 2 (a)).

Comparison of mean current speeds of the different grid resolution models (Fig. 2 (b)), suggest that the 15 m, 25 m, and 45 m predictions are similar. Mean velocity predictions of the larger node separation models (65 m, 85 m and 105 m), however, show considerable deviation from those of the higher resolution. The mean velocity standard deviations of the 25 m and 45 m lower resolution models compared to the 15 m node separation model, are 0.03 m/s and 0.05 m/s, respectively. For the lower resolution models, however, this rises to 0.13 m/s, 0.16 m/s and 0.18 m/s for the 65 m, 85 m and 105 m resolution models respectively. These results suggest that, at this water depth, a node separation of 45 m is preferable.

Fig. 2 (c) contains the standard deviation of the instantaneous current velocity from the same 10 stations. The figure suggests much less variation between the velocities predicted by the different resolution models (compared to the mean current velocity standard deviations). However, at the stations where high current velocities persist i.e. stations 1, 2 and 4, located on the bank crests in relatively deep water, there is an apparent jump (or reduction) in the standard deviation from the 45 m to 65 m resolution models, confirming the results inferred from the mean current analysis above.

3.2. Choice of model domain size

The next test focuses on minimising the size of the modelling domain. The argument in favour of using a large macro-scale model in the Bristol Channel is that it can provide a better description of the regional sediment fluxes: The hydrodynamics has more time and space to adjust to the dynamic forcing and reach an equilibrium state that is representative of the real conditions. In this study, very few observational data are available from which to derive a sediment flux boundary condition; indeed, it is one of the aims of the modelling exercise to determine the net flux into the system. The recursive nature of this problem is resolved by consideration of the sediment properties: Medium and coarse sand particles are transported, primarily, as bed load when current speeds exceed a well-defined threshold in either the flood or ebb directions (Lanzoni and Seminara, 2002). Suspension of sediment typically occurs during peak flood and ebb periods where entrainment and transport respond instantaneously to the fluid velocity, displaying almost zero lag between them (Dyer, 1986). Therefore, medium sand (250 μm to 500 μm) has little transport 'memory' and follows the current velocity closely. Flow asymmetries, characterized by shorter flood duration and higher flood current

maximum (i.e. flood dominance), induce an up-estuary directed sediment transport. Conversely, shorter ebb periods and greater ebb current maxima (ebb dominance) cause a net seaward directed sediment transport in the absence of wind and/or waves (Dronkers, 1986).

The above argument is derived in order to propose the use of a curtailed regional model of the Bristol Channel, its western boundary extending to a line connecting Bull Point with the Gower Peninsular (see Fig. 3). It is also assumed that, given an adequate model warm-up period, the system will achieve an equilibrium sediment concentration that is representative of the regional conditions. To validate this, two grids are tested including a larger regional domain and a smaller curtailed domain, the western boundary of which is detailed by the white dashed line in Fig. 3.

A particularly energetic period of wave action was selected from February 2004 in which wave heights exceeded 4 m (H_s) and wave periods were in the range of 9 to 18 s (T_{peak}) (4 month return period). The experiment consisted of the following steps:

1. An initial hydrodynamic model simulation was run using deep water tidal constituents (Andersen, 1995) defined at the western boundary at a resolution of 0.25°;

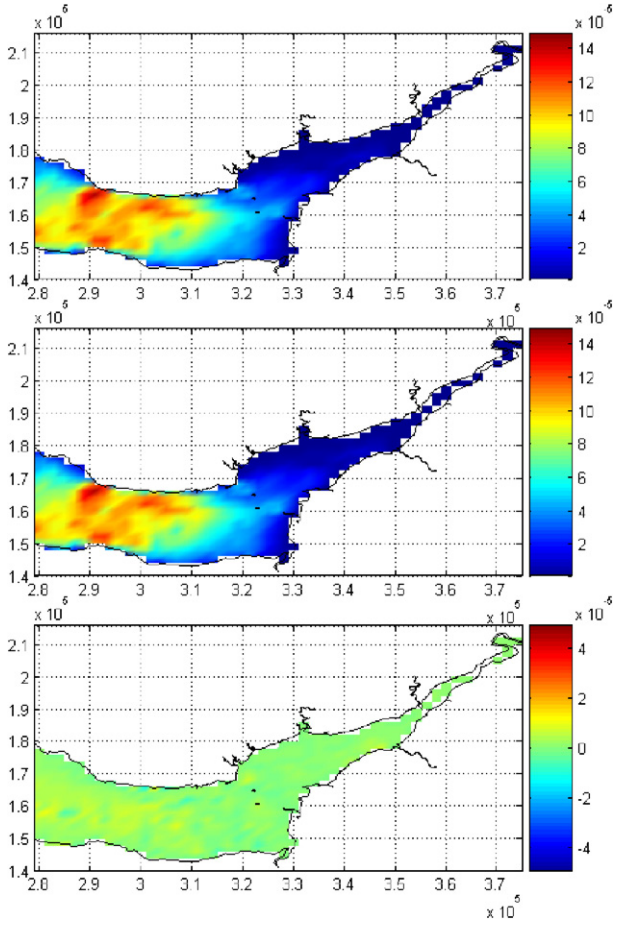

Fig. 4. Predictions of total load magnitude summed over one tide for: (a) the large model domain, and (b) the curtailed model domain. (c) Difference in total load magnitude summed over one tide predicted by the two models. Units are m^3/m.

2. A wave simulation was run using the large computational grid over the dynamic water levels and currents computed in Step (1). This provided an unsteady radiation stress field that varied due to both the external wave forcing and the internal water levels and currents;
3. A final coupled flow and sediment transport model was run over the same period utilising the radiation stress field and integral wave parameters previously computed in Step (2) to drive the sediment transport.

The same procedure was then repeated using the curtailed computational mesh. Gross sediment transport over one tide for the large and curtailed model domains have been plotted in Fig. 4 (a) and (b) respectively. The difference between the large and curtailed model gross transport predictions is plotted in Fig. 4 (c). The results demonstrate that there is a negligible difference between the large and the curtailed model predictions. The overall difference in the gross transport predicted by the two models is only 2.2%.

In addition to examining the spatial difference in the gross transport predicted by the two models, predictions at coastal locations, where there exist strong non-linear effects due to wave–current interaction, were also examined. Ten locations at which the water depth was less than 10 m were selected (see Fig. 5) and the predictions from both models were compared. The results, suggested a difference in the predicted gross transport of less than 10% (see Fig. 6), demonstrating that the use of a curtailed model is adequate. The tests also confirm that the prescription of an initial boundary flux is not a requirement because of the equilibrium character of the sediment transport in this particular situation.

4. Wave model optimisation

The DS model removes time as a dependent variable and solves the wave action-balance equation as a steady state solution (Holthuijsen et al., 1989). This parameterisation is based on the assumption that the propagation time of waves through coastal regions is short compared to the scale of wind and current fields. The DS model is further simplified by parameterisation of the frequency space in terms of a ‘directional action spectrum’ and a ‘mean wave frequency’. These are incorporated into the wave action-balance equation as functions of the spectral direction. The method retains the directional properties of the wave spectrum (considered important in coastal regions) but makes a simplification in the frequency space. The ‘directional action spectrum’ and the ‘mean wave frequency’ are functions of the zeroth and first moments of the action spectrum. Integration of these moments over the frequency of the wave-action spectrum provides spectral dependency of the wave propagation in the DS model (see Holthuijsen et al., 1989; Sørensen et al., 2004). The two parameterisations reduce the number of degrees of freedom from 125 to 25, and provide a 5-fold decrease in run time of the DS model compared to a full spectral wave model. It is desirable, therefore, to employ a DS model in this computationally intensive investigation. In the following test, the performance of the DS model is tested against measurements.

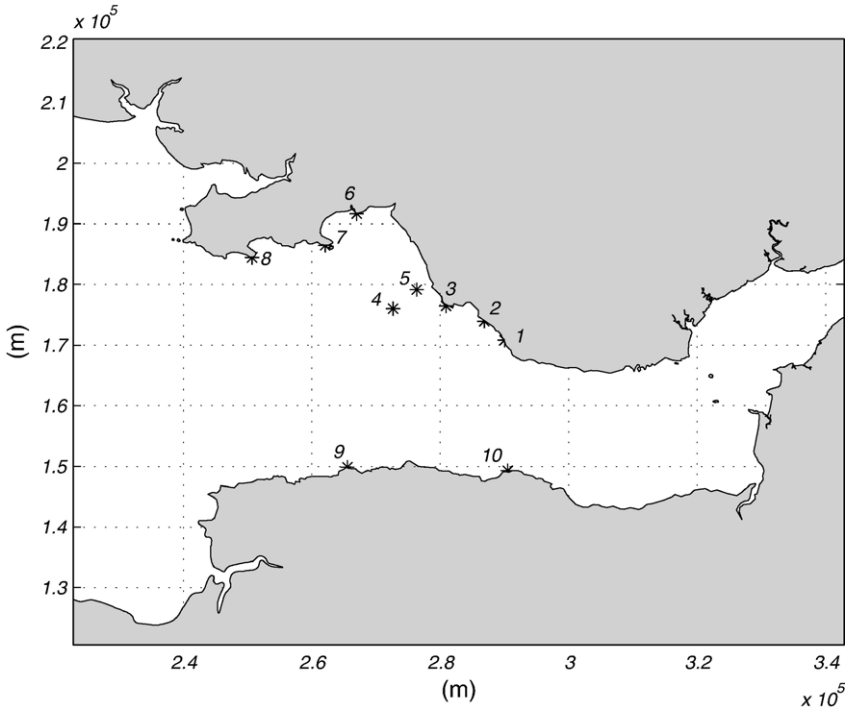

Fig. 5. Locations of the near-shore locations from which local values of total sediment transport were compared.

4.1. Validation of a parameterised wave model

A larger model domain (detailed in Fig. 3) is used to validate the DS model. The choice of this domain ensures that the position of the western boundary coincides with that of the Lundy Wavenet wave-rider buoy (51.17° N, 5.42° W, Cefas, 2002), from which real time-series directional wave data is available. A particularly energetic period of wave action from February 2004 (return period of 4 months) was selected as a driving boundary condition. Wind data extracted from Scar-weather wave-rider buoy (51.39° N, 3.91° W, U.K. Met. Office, 2005) over the same period is applied uniformly across the domain.

Wave simulations are performed by propagating a time-series of wave energy from the Lundy wave-rider buoy over a dynamic water level and current field. Wave-action transformations in the frequency domain are a result of changes in the bottom topography, wind field, ambient current and also from wave breaking (computed using the functional form of Ruessink et al., 2003). The performance of the model is assessed by comparing predictions of integral wave parameters with measurements at a wave-rider buoy in the upper Bristol Channel

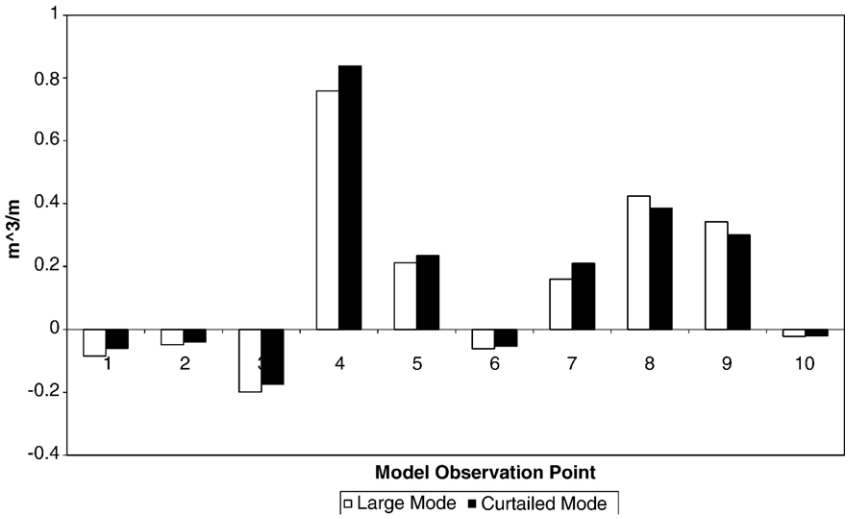

Fig. 6. Comparison of the total load sediment transport averaged over one tide at the near-shore locations indicated in Fig. 5.

(see Fig. 9 (a) for position) and comparing with measurements. Results (see Fig. 7) show good correlation between model predictions and measurements of significant wave height and peak wave period, providing sufficient evidence in support of using a more efficient DS model in the study.

4.2. Minimising the radiation stress field updating frequency

The modelling approach incorporates the effect of waves on sediment transport both directly via the *STPQ3* intra-wave sediment transport model and indirectly via the effect of radiation stresses on hydrodynamics (see Fig. 1). In dynamic environments, the radiation stress field will change considerably throughout a single tidal cycle due to the effects of changing water levels and currents. The following experiment demonstrates the effect of the tide on the wave-induced sediment transport around the Nash Sands using a small-scale local model of the region. The model is driven purely by a radiation stress field computed by propagating a wave field of 5 m (H_s) and 12 s (T_p) (propagating from west to east) over

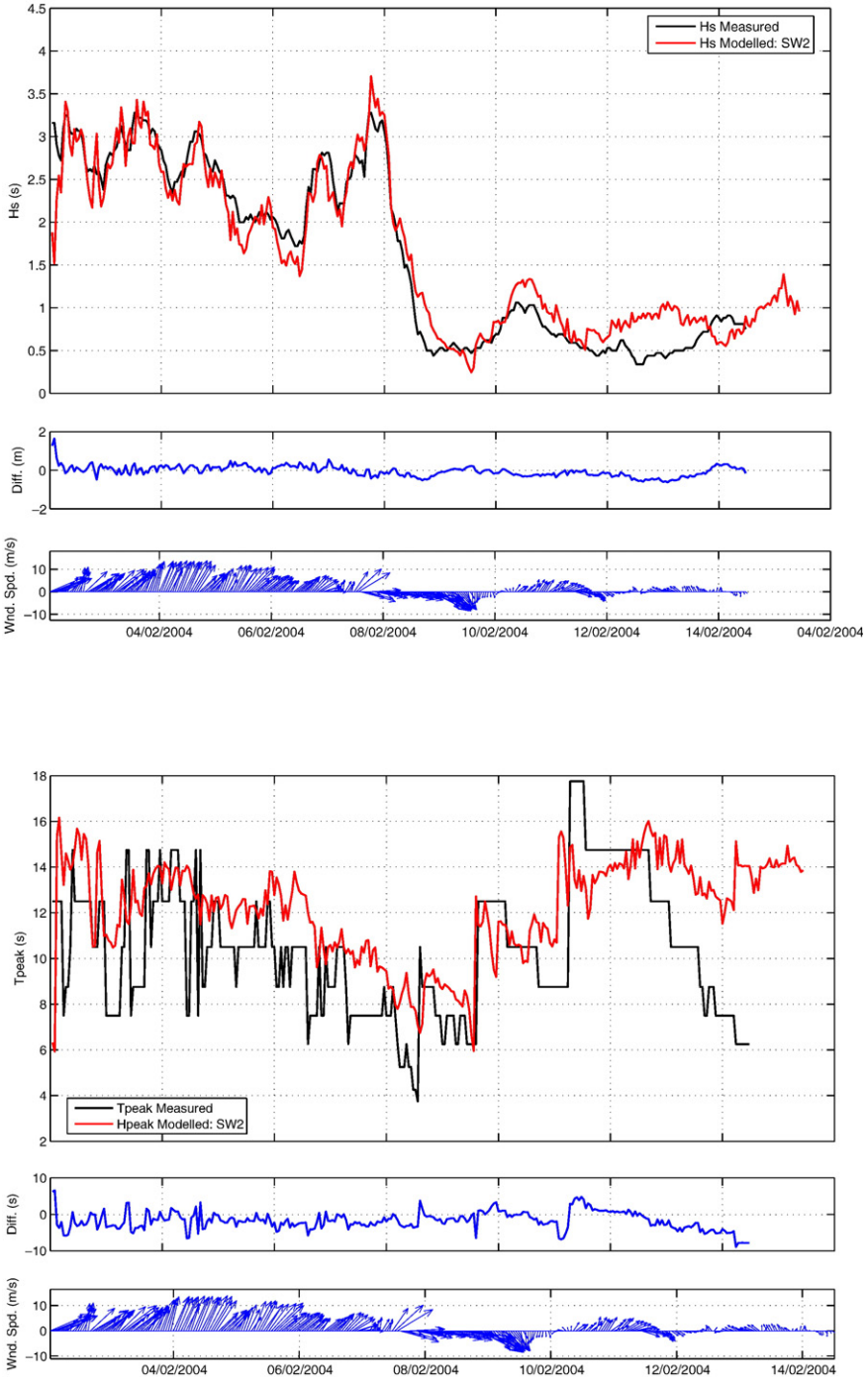

Fig. 7. Comparison of measured and modelled (a) significant wave height, and (b) peak wave period. Also plotted are time-series of calculated difference and wind speed/direction.

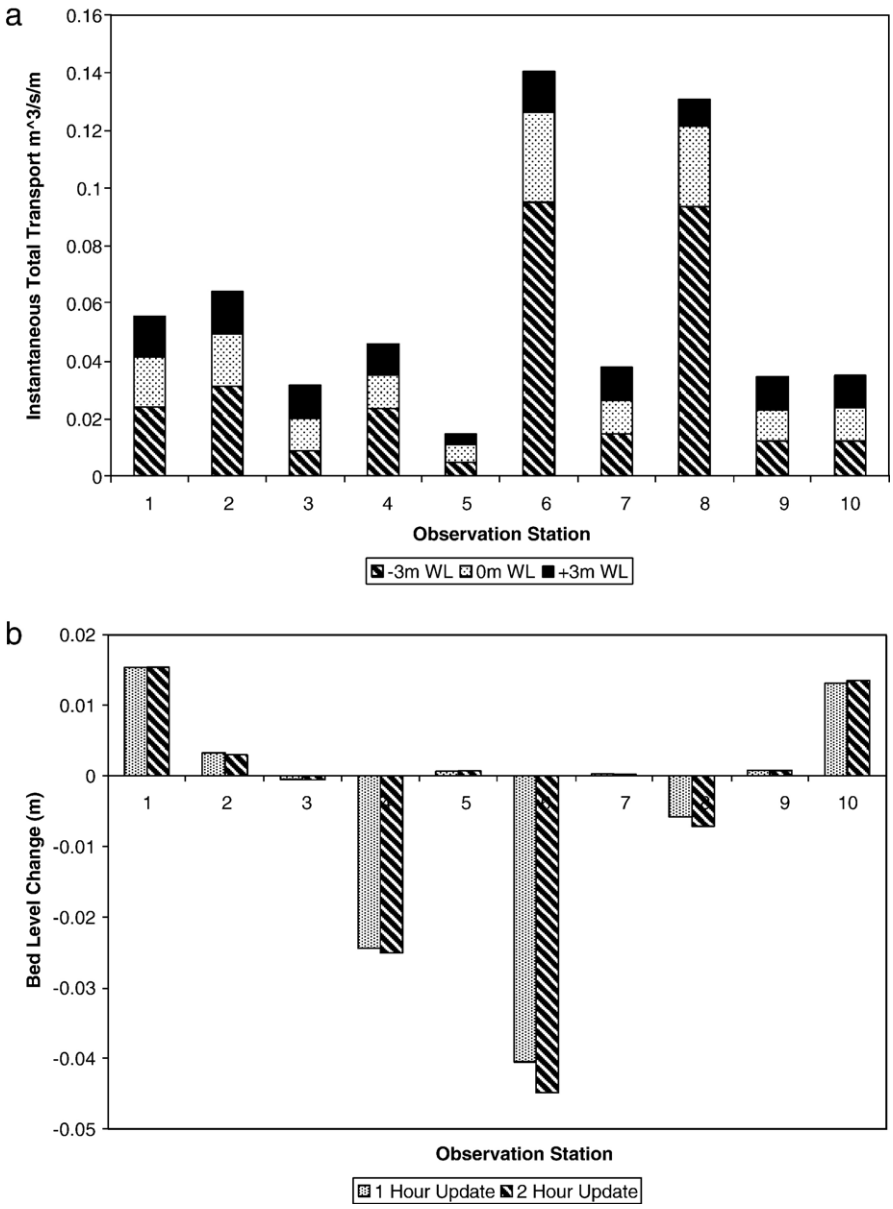

Fig. 8. (a) Total load transport and (b) bed level change predicted at 10 observation points under a 2 m (H_s), 10 s (T_{peak}) monochromatic waves for three tidal levels.

three different ambient conditions. The water depth of the observation sites varies from 2 to 15 m (see Fig. 2 (a)).

The predicted rates of sediment transport (Fig. 8 (a)) suggest that a decrease in water depth of 3 m can be related to a doubling in the sediment transport rates. The effect is even greater in shallow-water locations. For example, at observation stations 5 and 6 situated at the crest of the sandbank, the predicted sediment transport increases by more than a factor of 3 for a reduction in water depth of 3 m. In addition to highlighting the importance of computing the radiation stresses on a dynamic water level, the test also highlights the need to re-compute radiation stresses a number of times within a complete tidal cycle. This idea is developed further in the next section.

Radiation stresses are computed at two intervals of 60 and 120 min over a spring tide using the DS wave model and curtailed mesh validated in Sections 4.1 and this section. The resulting radiation stress fields are then utilised by the coupled HD/ST model.

Results from the two tests suggest that increasing the updating interval from 60 to 120 min has only a limited impact on predictions. Comparisons of bed-level changes from point locations at the Nash Sands (see Fig. 8 (b)) suggest only a fractional adjustment (maximum of 0.005 m). The difference is relatively minor, given that the test has been conducted under strong forcing conditions (spring tides and 5 m waves). The effect on the regional sediment transport is also negligible: Comparison of the gross sediment transport at two cross-

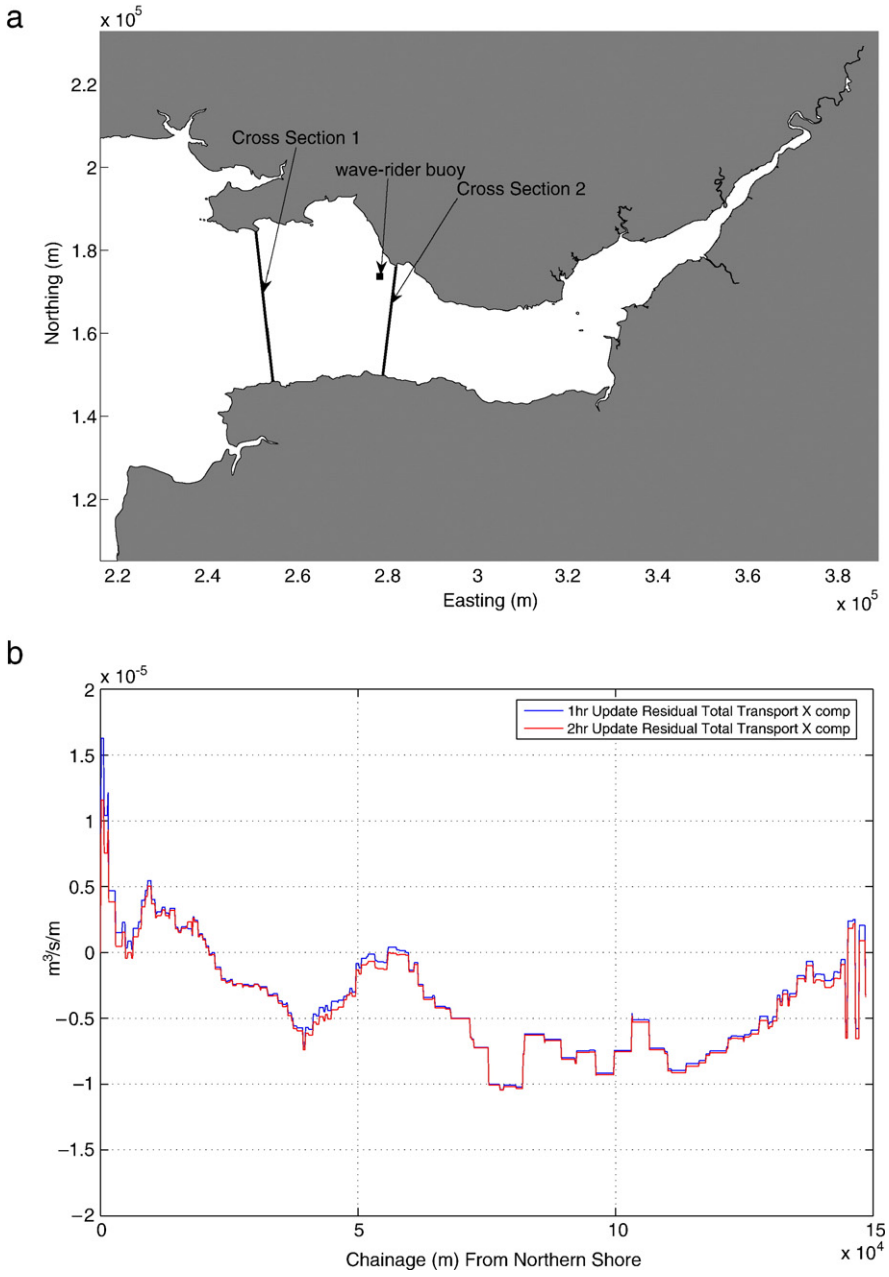

Fig. 9. (a) Positions of 2 cross-sections at which mean total load transport is computed. (b) Westerly component of residual total load transport from cross-section 1 (see Fig. 5) computed over 1 tidal cycle.

sections (see Fig. 9 (b) and (a) for positions) demonstrates an almost unnoticeable difference in the predicted transport. The results suggest that a relaxation of the updating interval, from 60 min to 120 min, is acceptable in this situation.

5. Optimising the sediment transport/morphological models

5.1. Updating frequency

Under most conditions, changes to the sediment transport and morphology are slow in comparison with those of the hydrodynamics (van Rijn, 1993). Intuitively, this suggests that it

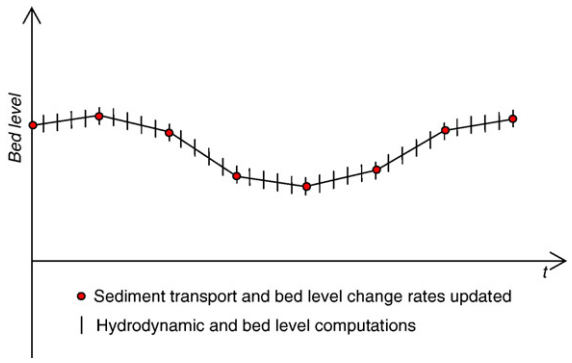

Fig. 10. Procedure used to reduce the number of calls to the sediment transport/morphology modules.

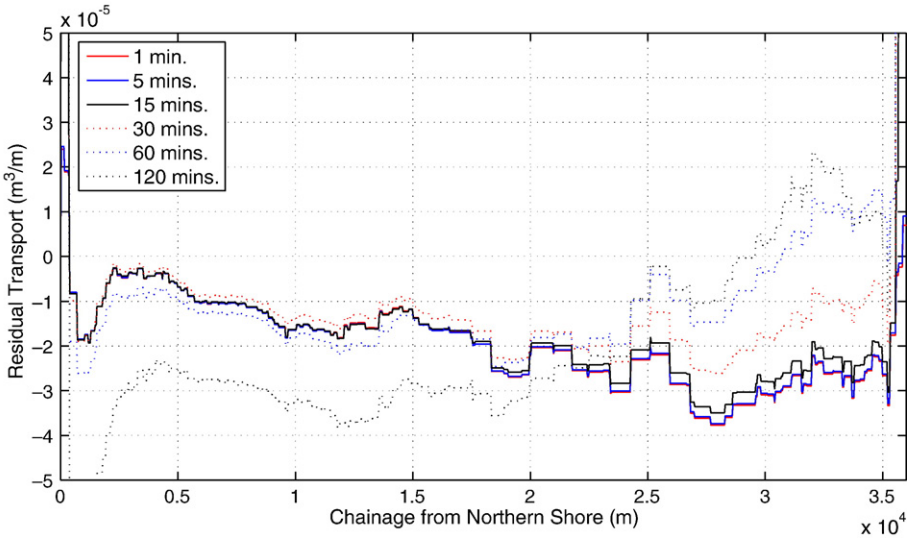

Fig. 11. Residual sediment transport (westerly component) for varying sediment transport updating intervals, over 1 complete spring tide from cross-section 1 (see Fig. 5).

is possible to limit the number of calls to the computationally expensive sediment transport and morphological modules to a specified frequency of the hydrodynamic computations. The coupled model employed in this study uses an explicit Euler scheme to update the sediment transport at every 'morphological time-step' (see also Fig. 10),

$$q^{n+1} = q^n + \frac{\mathrm{d}q}{\mathrm{d}t}|_n \Delta t \tag{4}$$

where q^n and q^{n+1} are the sediment transport rates at the current and next time-steps respectively, $\mathrm{d}q / \mathrm{d}t$ is the rate of sediment transport or bed-level change. Δt is the time difference between successive calls to the sediment transport/morphological models. In the following experiment, the applicability of this scheme is tested in the Bristol Channel, where the interaction of waves and currents provides the potential to generate non-linear flow fields and sediment transport.

Using the regional model grid (Fig. 3) and a radiation stress field from a 5 m (H_s) wave computed on a stationary water level, 6 coupled hydrodynamic/sediment transport simulations were performed that each used a different number of calls to the sediment transport model over a complete tidal cycle. The updating intervals tested are 1, 5, 15, 30, 60, 120 mins. The aim of the experiment was to obtain an updating interval that is both accurate and computationally efficient. It is assumed that the most accurate description of the sediment transport is provided by the lowest updating interval. The accuracy of the remaining updating intervals will therefore be measured by comparison to the 1 minute interval predicted transport rates.

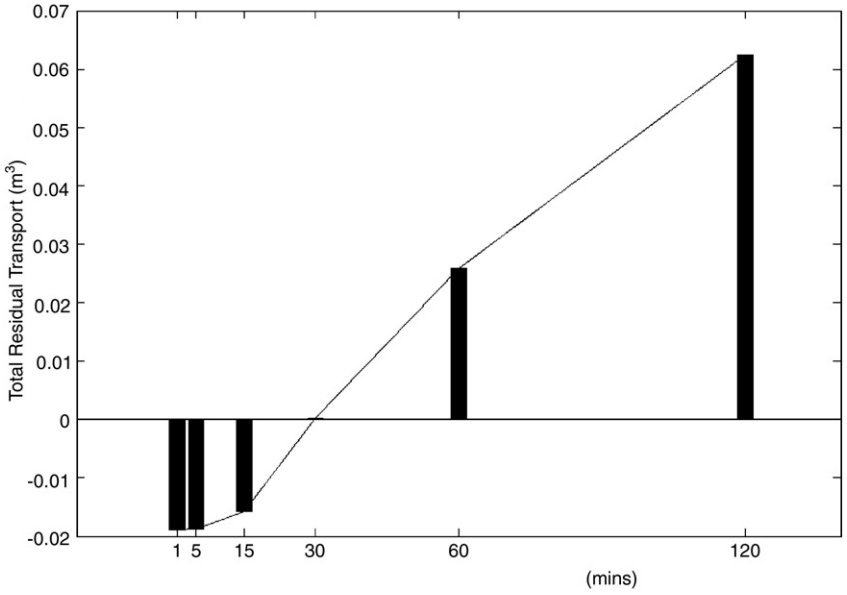

Fig. 12. Residual transport integrated over cross-section 1 for 6 different updating intervals.

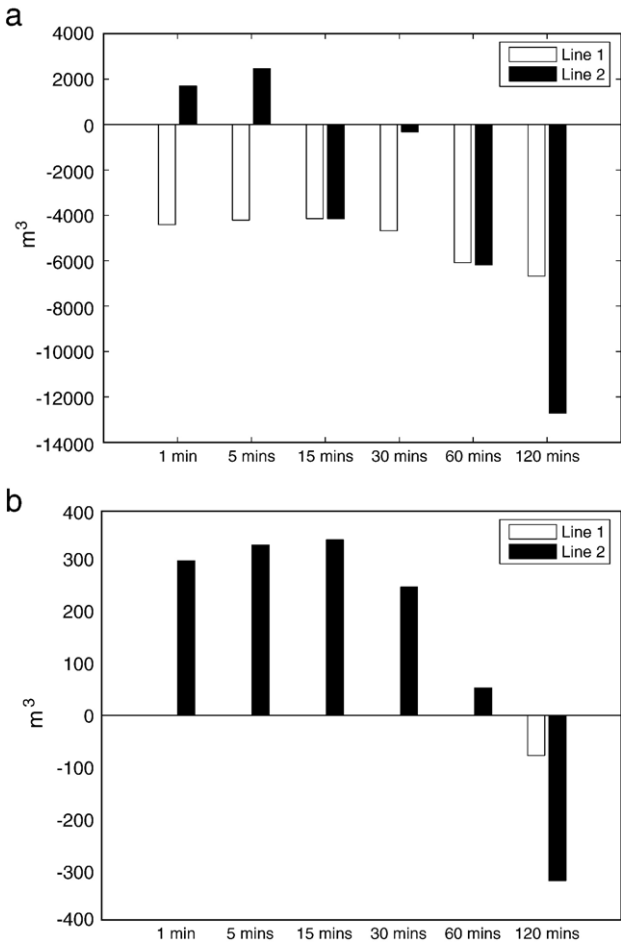

Fig. 13. Predictions of total load sediment transport over 1 spring tide at cross-sections 1 and 2 for grain sizes of (a) 150 μm and; (b) 270 μm.

Fig. 11 demonstrates that the predicted sediment transport is extremely sensitive to the updating interval. Both the 5 and 15 minute updating intervals predict residual sediment transport that is comparable to the 1 minute updating interval test. However, an increase of the updating interval above 15 min is accompanied by a significant difference in both the pattern of residual transport across the estuary and the total transport computed over a tide (see Fig. 12). This suggests that in order to resolve both the inter-tidal dependency of the wave-induced currents, and the equilibrium response of the sediment transport to the ebb-dominated tidal currents, a low updating interval is required. The use of a minimum 15 minute updating interval is, therefore, recommended for subsequent modelling experiments in this environment.

Table 1
Dependency of sediment transport updating interval on grain size

Updating frequency (/min)	1	5	15	30	60	120
270 μm; line 1	1.0000	0.9422	0.9047	1.0306	1.1353	0.2768
270 μm; line 2	1.0000	0.9695	0.9607	0.3032	1.1004	0.4496
150 μm; line 1	1.0000	1.0235	1.0340	0.9792	0.8193	0.7474
150 μm; line 2	1.0000	0.9829	−1.2695	−1.1481	0.9624	0.6464

5.1.1. The effect of grain size on the sediment transport updating frequency

Additional tests were also conducted to establish the dependency of the updating interval on the grain size. Two grain sizes were selected, 150 μm and 270 μm, both present in large quantities within the study (based on BGS, 1986). Transport tables were computed for these two sediment sizes using the *STPQ3* model and the combined wave-flow model

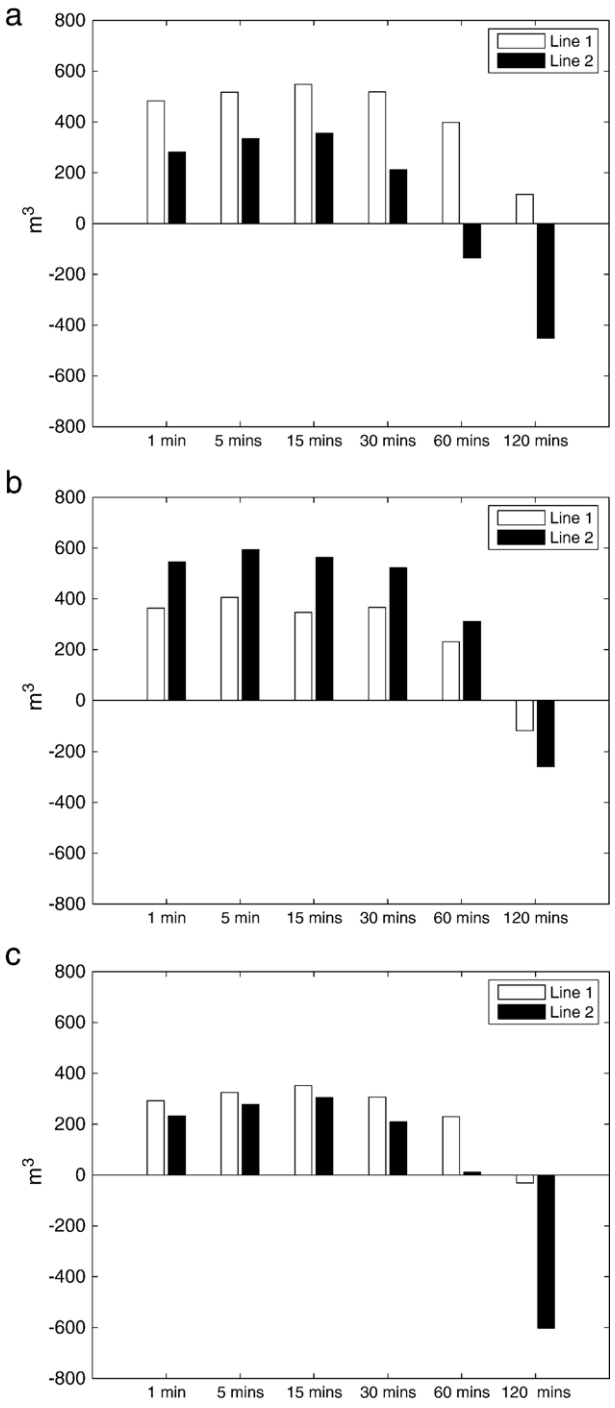

Fig. 14. Predictions of total load sediment transport averaged over 1 spring tide at cross-sections 1 and 2 for wave heights of (a) 1 m; (b) 3 m and (c) 5 m.

was re-run over a spring tidal period using a uniform wave of 2 m (H_s) and 9 s (T_{peak}) defined at the western boundary. The radiation stresses as well as the integral wave parameters were therefore both subject to dynamic water levels and currents.

Total load transport averaged over one tide was extracted from two cross-sections (see Fig. 9 (a) for positions) and integrated across the estuary. The total volume transport predicted for the two grain sizes (at both cross-sections) is presented in Fig. 13 (a) and (b).

For the 150 μm case, the predicted transport direction at cross-section 2 reverses between the 5 minute and the 15 minute updating intervals. This shows that, for this grain size, a relatively low updating interval is required (at least 5 min) in order to capture the reversal in the transport direction predicted by the 1 minute updating interval model.

For the experiments involving the larger 270 μm sand grains, the mean transport direction predicted at both cross-sections 1 and 2 is eastward for the 1 minute, 5 minute, 15 minute, 30 minute and 60 minute cases, suggesting that the lower updating intervals are able to reproduce the transport directions adequately for this grain size. However, the accuracy of the lower interval results (30 min and 60 min) compared to the 1 minute case, is much less. Table 1 presents ratios of the total transport averaged over one tide predicted by the 1 minute model runs to the other five updating intervals. Uncertainty in the model predictions can be measured by the extent to which the ratios differ from a value of 1. Increasing uncertainty is detected as the updating interval increases and the grain size reduces.

Overall, the results suggest that as the grain size reduces, the updating interval prescribed by the user must increase to accommodate the additional time in which the smaller sediment fractions remain suspended in the water column after periods of peak current velocity.

5.1.2. The effect of wave height on sediment transport updating frequency

The sensitivity of the updating interval to wave height was also tested. Waves of 1 m, 3 m and 5 m (H_s) and period of 9 s (T_{peak}), were propagated from the western boundary of the model during a single spring tide. The total load transport averaged over one tide, predicted at cross-sections 1 and 2, is presented in Fig. 14 (a), (b) and (c) for the 1 m, 3 m and 5 m wave conditions respectively. The ratios of the total transport predicted after 1 tide by the 1 minute model run to the other five updating interval tests are presented in Table 2. Again, the uncertainty in the results (relative to the 1 minute updating interval) increases with the updating interval (for all wave conditions), however, no clear relationship exists between the maximum permissible updating interval and the wave height.

5.2. Morphological acceleration factor

A further technique, aimed at improving the efficiency of longer-term morphological predictions, is to apply an acceleration factor to the bathymetry changes. At each call to the morphological model, the bed-level change rate is multiplied by a factor, MFAC

$$z^{n+1} = z^n + \left[\frac{\mathrm{d}z}{\mathrm{d}t}|_n \times \mathrm{MFAC} \times \Delta t\right] \quad (5)$$

The validity of applying a morphological scaling factor (henceforth, MFAC), however, is strongly dependant on the difference in time-scales between the hydrodynamic forcing and the bed changes. In low energy environments where morphology evolves slowly (and linearly) in response to more constant forcing, a high MFAC is appropriate because there is less ambiguity in the feedback between the changing bed and the hydrodynamics. However, under stronger forcing, non-linear bed evolution requires more careful selection of an appropriate MFAC. Some approaches (e.g. van Ormondt et al., 2005) adjust the scaling factor depending on the severity of the forcing, using progressively smaller factors with increasing wave action. The choice of the scaling factor, however, is based on only an a-priori assessment of the likely magnitude of the bed change rate induced by various forcing conditions. The strong tidal and wave forcing present in the Bristol Channel means that reliable application of a MFAC requires a prescient knowledge of its limitations. Therefore, in this study, a number of simulations have been conducted to test the use of a MFAC under varying hydrodynamic forcing conditions. Using the curtailed modelling domain (see Fig. 3) to facilitate longer-term simulations, the bed change predicted over 41 tidal cycles using scaling factors of 1, 2, 5, 10, 25, 50 and 100 is extracted. The same tests are then performed with increased forcing provided by a 1 m 9 s wave and 2 m 9 s wave. The aim of the test is to determine the point at which each MFAC becomes unreliable under different forcing conditions. The following criteria are assessed: stability and adherence to linearity.

The model time-step is limited by a Courant–Friedrichs–Levy (CFL) number condition of 1 due to the explicit numerical scheme which restricts the amount of bed-level change that can occur over the fixed time-step. In the experiments it was found that, when using combinations of large MFACs and strong forcing conditions, model stability became an issue. When testing MFACs of above 25, it was necessary to limit the rate of change of the bed level per time-step, in order to prevent the CFL number from exceeding stable limits.

Reliable application of the MFAC also relies on the assumption that bed changes predicted at one time-step can be multiplied linearly. However, feedback between the changing

Table 2
Dependency of sediment transport updating interval on wave height

H_s=1 m; line 1	1.0000	0.9531	0.9126	0.9577	1.1222	1.4922
H_s=1 m; line 2	1.0000	0.9763	0.9662	1.0216	0.8894	0.5594
H_s=3 m; line 1	1.0000	0.9215	0.9870	0.9656	1.0815	0.2331
H_s=2 m; line 2	1.0000	0.9580	1.0075	1.0046	1.1661	0.4701
H_s=5 m; line 1	1.0000	0.9678	0.9310	0.9431	0.9037	0.6791
H_s=1 m; line 2	1.0000	0.9774	0.9574	0.9892	0.9770	0.4280

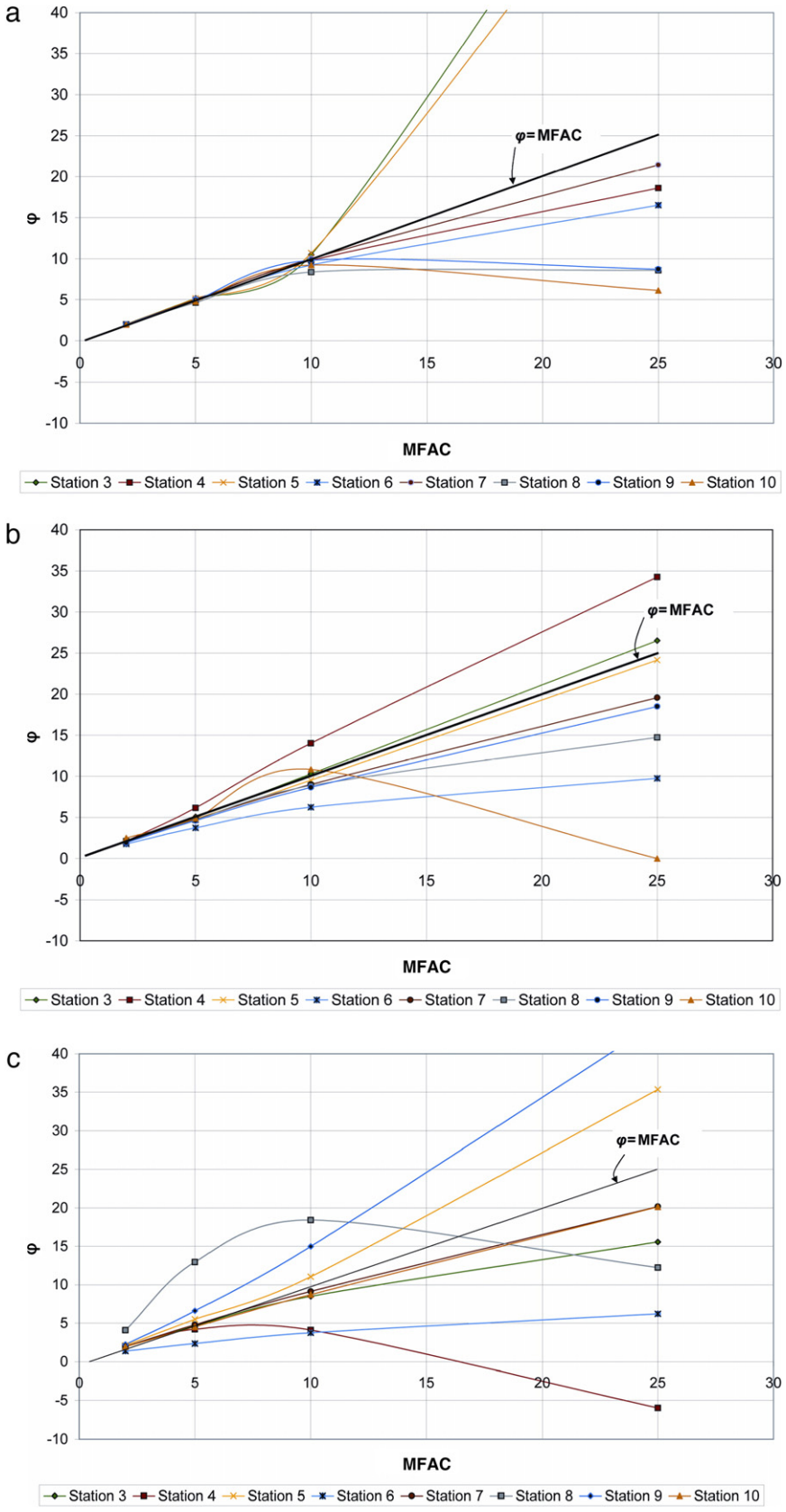

Fig. 15. MFAC plotted against the ratio of final bed changes predicted using a MFAC to final bed changes predicted using no MFAC for conditions of (a) tides alone; (b) tides+1 m, 9 s waves and; (c) 2 m, 9 s waves.

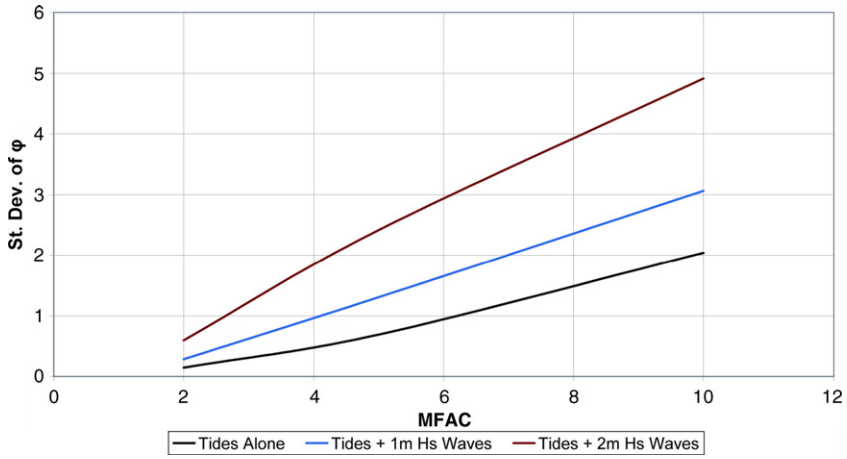

Fig. 16. MFACs plotted against the standard deviation of φ for different forcing conditions.

bed and the hydrodynamics means that under strong forcing conditions, this assumption becomes invalid. The following analysis attempts to find a reliable range of MFACs that can be applied in a given set of forcing conditions. A test criterion, φ, is computed from the model results as a method of measuring the linearity of the bed changes predicted under each test condition, where

$$\varphi = \frac{dz_{MFAC^n}}{dz_{MFAC^1}} \tag{6}$$

dz is the bed change at the end of each simulation predicted using a MFAC of n(n=2, 5...100). If the bed responds linearly to the forcing, φ must be equal to MFAC^n. The deviation of φ from MFAC^n, gives an indication of the non-linear behaviour of the system and an upper limit at which the MFAC can be applied reliably. We compute the value of φ at a number of observation positions (detailed in Fig. 2 (a)) for each test (see Fig. 15 (a), (b) and (c)).

For all three conditions (tides alone, tides+1 m waves, tides +2 m waves), as the value of the MFAC is increased, the predicted bed changes begin to deviate away from the ideal condition of φ=MFAC. As the forcing is increased, the deviation occurs at increasingly lower values of MFAC. For the tides alone scenario, significant deviation from linearity occurs at MFAC=10. For the 1 m and 2 m wave scenarios, significant deviation occurs at MFAC of 5 and 2, respectively.

In order to provide a spatially integrated demonstration of the breakdown of the linear assumption with increasing forcing and MFAC, the standard deviation of φ at all observation positions (Fig. 16) has been computed. The results show that at larger MFAC and under stronger forcing, the deviation increases. If a standard deviation of 1 is chosen as a cut-off point for applicability, then under high spring tides, we are limited to a MFAC of approx. 6. This reduces to MFAC of 4 and 2.5 for 1 m, 9 s and 2 m, 9 s waves, respectively, confirming that morphological factors need to be used cautiously in dynamic environments.

An alternative to the MFAC approach described here, also used to save computational time, is the 'continuity correction'. This approach assumes that the flow will not be affected by small changes to the bathymetry and in between calls to the hydrodynamic module, the flow rate from the last hydrodynamic computation is used to solve the sediment balance equation and update the bed incrementally. When the bed changes exceed a pre-defined level, an update to the hydrodynamics is triggered. The approach mitigates the problems associated with non-linearity by ensuring that an update is triggered by abrupt or significant bed changes rather than being restricted to a fixed interval (as in the MFAC approach). The problem with the 'continuity correction' approach is that is assumes that the flow rate and pattern remain constant between morphological updates which, for a channel or feature that is becoming increasingly shallow, is clearly not true. The approach also requires full sediment transport computations to be made in between calls to the hydrodynamic module which may be computationally demanding if a lot of suspended sediment is present. Another problem with the approach is that the morphological time-step is always controlled by the most shallow grid cells which are usually not of interest. Introducing a 'non-fixed' speed-up factor would provide the advantages of both the MFAC and 'continuity correction'. However, the question remains as to how to control the speed-up factor and link it to the 'real world' not only for a point but for the entire domain.

6. Summary and conclusions

The experiments carried out in this study have provided a model setup that can be applied in a large-scale, regional study where important wave and current processes occur at a variety of spatial scales. The model has been optimised at a number of levels. Initially, an ideal mesh resolution was established by assessing the dissipation of sub-grid level energy by model domains of varying resolution. The results suggested that a 45 m node separation model produces similar current fields to a 15 m

node separation model in this environment. This demonstrated the validity of the turbulence closure scheme at the lower resolution and provided justification for using a 45 m node separation model in subsequent experiments. Further improvement of the computational efficiency was then added by reducing the spatial footprint of the mesh. Comparisons of regional sediment transport and local bed changes demonstrated the equilibrium character of the regional sediment transport and hence, provided evidence to suggest that a smaller (and therefore more efficient model) was capable of resolving large-scale transport processes in sufficient detail.

A number of tests were then performed to improve the efficiency of the model coupling. By restricting the number of calls to expensive parts of the flow or wave models, the radiation stress field and the sediment transport updating intervals were optimised. Under high wave and tidal forcing it was shown that a radiation stress field updating interval of 120 min is sufficient to capture adjustments made to the wave-induced current field by a dynamic tide in this environment. Attempts to optimise the sediment transport rates under similar forcing, however, suggested that at least a 15 minute updating interval is required.

Finally, a set of morphological acceleration factors were derived for different forcing conditions. By testing a range of MFACs, the model stability and adherence to linearity of the predicted bed changes were assessed. Results demonstrated that when using a MFAC above 25, stability is severely limited under all driving conditions. To test the validity of the linear assumption, a dimensionless number φ was computed which measured the ratio of bed changes at a given MFAC to bed changes predicted using no MFAC. Deviation from a condition of φ=MFAC indicated a breakdown of the assumption of linearity. For a range of forcing conditions, it was found that with increasing forcing conditions, the MFAC at which the condition is violated reduces.

Overall the experiments demonstrated that consideration and understanding of the dynamics of a region is helpful in order to select model parameters that accurately describe the physical processes. Relaxation of the model coupling should be performed carefully with numerous test simulations being conducted in order to assess whether the contributing processes are being captured properly. In the above scenario, the primary interest was combined wave/current induced sediment transport which required simulation of the complex regional tidal currents and wave-induced currents in shallow-water areas. The results presented aim to provide some direct guidance to modellers/coastal engineers working in comparable environments that are subject to both high tidal and wind/wave energies. Although the settings and optimisations may not be directly transferable to all situations, the study provides a methodology as to how the validity of the many assumptions and shortcuts required in real coastal modelling projects can be tested.

Acknowledgements

The authors are grateful to Drs. H. Johnson and O. S. Sørensen for useful discussion and advice and also to the EPSRC for financial support to the first writer.

References

Abbott, M.B., Minns, 1998. Computational Hydraulics. Ashgate Publ. Ltd. 557 pp.

Andersen, O.B., 1995. Global ocean tides from ERS-1 and TOPEX/POSEIDON altimetry. Journal of Geophysical Research 100 (C12), 25249–25259.

Bakker, W., Van Doorn, T., 1978. Near bottom velocities in waves with a current. Proceedings of the 16th Coastal Engineering Conference, vol. 2, pp. 1394–1413.

B.G.S., 1986. Sea Bed Sediments and Quaternary Geology: Bristol Channel Sheet 51N-04W. HMSO, London.

Cefas, 2002. WAVENET Directional Wave Data from 'Lundy wave-rider buoy'. 51.16 N 5.34 W; 27/01/04–21/04/05.

de Vriend, H.J., Capobianco, M., Chesher, T., de Swart, H.E., Latteux, B., Stive, M.J.F., 1993. Approaches to long-term modelling of coastal morphology: a review. Coastal Engineering 21, 225–269.

DHI, 2005. MIKE 21/3 Flow Model FM Hydrodynamic and Transport Module Scientific Documentation. DHI Group, Horshølme.

Dyer, K.R., 1986. Coastal and Estuarine Sediment Dynamics. Wiley, Chichester, U.K., 342 pp.

Dronkers, J., 1986. Tidal and estuarine sediment dynamics. Netherlands Journal of Sea Research 20 (2/3), 117–131.

Fredsøe, J., 1984. Turbulent boundary layers in wave–current motion. Journal of Hydraulic Engineering, ASCE 110 (HY8), 1103–1120.

Harris, P.T., Collins, M.B., 1985. Bedform distributions and sediment transport paths in the Bristol Channel and Severn Estuary, U.K. Marine Geology 62, 153–166.

Harris, J.M., Jones, O.P., 2005. Modelling the effect of wave current interaction on sediment transport in the Bristol Channel U.K. Proceedings of Waves 2005, Madrid, Spain.

Holthuijsen, L.H., Booij, N., Herbers, T.H.C., 1989. A prediction model for stationary short-crested waves in shallow water with ambient currents. Coastal Engineering 13, 23–54.

Hudson, J., Damgaard, J.S., Dodd, N., Chesher, T.J., Cooper, A.J., 2005. Numerical approaches for 1D morphodynamic modelling (In proof) Coastal Engineering.

Kemp, P., Simons, R.R., 1982. The interaction of waves and turbulent current: waves propagating with the current. Journal of Fluid Mechanics 116, 227–250.

Komen, G.J., Cavaleri, L., Doneland, M., Hasselmann, K., Hasselmann, S., Janssen, P.A.E.M., 1994. Dynamics and Modelling of Ocean Waves. Cambridge University Press, U.K., 560 pp.

Lanzoni, S., Seminara, G., 2002. Long-term evolution and morphodynamic equilibrium of tidal channels. Journal of Geophysical Research 107, C1.

Latteaux, B., 1992. Long-term morphological simulation under tidal current with non-cohesive sediment. MAST G6-M Final Workshop, Paper 5.18.

Leont'yev, I.O., 2003. Modeling erosion of sedimentary coasts in the western Russian Arctic. Coastal Engineering 47, 413–429.

Longuet-Higgins, M.S., Stewart, R.W., 1964. Radiation stress in water waves; a physical discussion, with applications. Deep-Sea Research 11, 529–562.

Roelvink, J.A., 2006. Coastal morphodynamic evolution techniques. Coastal Engineering 53, 277–287.

Ruessink, B.G., Walstra, D.J.R., Southgate, H.N., 2003. Calibration and verification of a parametric wave model on barred beaches. Coastal Engineering 48, 139–149.

SANDPIT, 2005. Sand transport and morphology of offshore sand mining pits. In: Van Rijn, L.C., Soulsby, R.L., Hoekstra, P., Davis, A.G. (Eds.), Aqua Publications, The Netherlands.

Smagorinsky, J., 1963. General circulation experiments with the primitive equations: I. The basic experiment. Monthly Weather Review 91, 99–164.

Sørensen, O.R., Kofoed-Hansen, H., Rugbjerg, M., Sørenson, L.S., 2004. A third-generation spectral wave model using an unstructured finite volume technique. ICCE 2004, Lisbon.

UKMO, 2005. Directional Wave-Data from the Scarweather Wave-Rider Buoy: 51.39° N 3.91° W; 01/06/2000–31/12/2004.

Van Ormondt, M., Walstra, D.J., van Rijn, L.C., Roelvink, D., Spanhoff, R., 2005. Optimising and understanding shoreface nourishments. In: Sanchez-Arcilla, A. (Ed.), Proceedings of the 5th International Confenrence on Coastal Dynamics. ASCE.

van Rijn, L.C., 1993. Principles of Sediment Transport in Rivers, Estuaries and Coastal Seas. Aqua Publications.

Notation

a_1: constant
h: characteristic length scale
H_s: significant wave height
Q: sediment transport
T_p: peak wave period
$\overline{S}$: shearing intensity
t: time
$\overline{u}_i$: horizontal velocity
$\overline{u}_j$: vertical velocity
V: ambient current velocity
x_i: horizontal coordinate
x_j: vertical coordinate
z^n: bed level at the current time-step
z^{n+1}: bed level at the next time-step
Δx_n: grid spacing
φ: dimensionless ratio
υ_t: turbulent eddy viscosity
τ_{ij}: internal fluid shear stress